Inorg. Chem. **2004**, *43*, 515–529

Supramolecular Recognition of Heteropairs of Lanthanide Ions: A Step toward Self-Assembled Bifunctional Probes

Nicolas André,[†] Thomas B. Jensen,[†] Rosario Scopelliti,[†] Daniel Imbert,[†] Mourad Elhabiri,[‡] Gérard Hopfgartner,[§] Claude Piguet,[||] and Jean-Claude G. Bünzli*,[†]

Institute of Molecular and Biological Chemistry, Swiss Federal Institute of Technology, BCH 1402, CH-1015 Lausanne, Switzerland, Laboratoire de Physico-Chimie Bioinorganique UMR 7509 CNRS, École Européenne de Chimie, Polymères et Matériaux, 25 rue Becquerel, F-67087 Strasbourg, France, and Laboratory of Pharmaceutical Analytical Chemistry, School of Pharmacy, University of Geneva, 20 bd d'Yvoy, and Department of Inorganic, Analytical and Applied Chemistry, University of Geneva, 30 quai E. Ansermet, CH-1211 Geneva 4, Switzerland

Received October 17, 2003

Three unsymmetrical ditopic hexadentate ligands coded for the recognition of trivalent lanthanide ions have been synthesized, L^{AB}, L^{AC}, and L^{BC}, where A represents a benzimidazole–pyridine–benzimidazole coordination unit, B a benzimidazole–pyridine–carboxamide one, and C a benzimidazole–pyridine–carboxylic acid moiety. Under stoichiometric 2:3 (Ln:L) conditions, these ligands self-assemble with lanthanide ions to yield triple-stranded bimetallic helicates having a sizable stability in acetonitrile: log β_{23} values for Eu are equal to 23.9 ± 0.5 (L^{AB}), 23.3 ± 0.7 (deprotonated L^{AC}), and 29.8 ± 0.5 (deprotonated L^{BC}). The crystal structure of the EuEu helicate with L^{AB} shows 9-coordinate metal ions and an HHH (H stands for head) configuration of the helically wrapped ligand strands. In the presence of equimolar quantities of Ln and Ln′ ions, L^{AB} displays a remarkable predisposition to form HHH-heterobimetallic edifices, as proved both in the solid state by the crystal structures of the LaEu, LaTb, PrEr, and PrLu helicates and in solution by NMR spectroscopy. In all cases, the benzimidazole–pyridine–carboxamide units of the three ligands are bound to the smaller lanthanide ion, a fact further ascertained by high-resolution luminescence data on LaEu and by ^{1}H NMR. Analysis of the lanthanide-induced ^{1}H NMR shifts and of the spin–lattice relaxation times of the $[LnLu(L^{AB})_3]^{6+}$ series (Ln = Ce, Pr, Nd, Sm, Eu) demonstrates the isostructural nature of the complexes in solution and that the crystal structure of LaTb is a good model for the solution structure. The selectivity of L^{AB} for heteropairs of Ln^{III} ions increases with increasing difference in ionic radius, resulting in 70% of the heterobimetallic species for $\Delta r_i = 0.1$ Å and up to 90% for LaLu ($\Delta r_i = 0.18$ Å), and corresponding to $\Delta(\Delta G)$ in the range 3–10 kJ·mol^{-1}. The origins of this stabilization are discussed in terms of the donor properties of the coordinating units and of the preferential formation of HHH isomers.

Introduction

New challenges in diagnosis and therapy have prompted interest in several aspects of lanthanide-containing probes, contrast agents, and drugs.[1] Well-established applications are the uses of trivalent erbium in the separation and isolation of bacterial or eukaryotic cells,[2] of trivalent gadolinium in magnetic resonance imaging,[3] or of the same ion in phosphors for X-ray-intensifying screens.[4] New developments include cancer radio- and phototherapy.[5] Optical probes also attract special attention for the following reason. The parity rule forbidding intraconfigurational 4f−4f transitions is only

* Author to whom correspondence should be addressed. E-mail: jean-claude.bunzli@epfl.ch.
[†] Swiss Federal Institute of Technology.
[‡] École Européenne de Chimie, Polymères et Matériaux.
[§] School of Pharmacy, University of Geneva.
[||] Department of Inorganic, Analytical and Applied Chemistry, University of Geneva.

(1) *The Lanthanides and Their Interrelations With Biosystems*, *Metal Ions in Biological Systems*; Sigel, A., Sigel, H., Eds.; Marcel Dekker Inc.: New York, 2003; Vol. 40.
(2) Evans, C. H. *Biochemistry of the Lanthanides*; Plenum Press: New York, 1990.
(3) Merbach, A. E.; Tóth, E. *The Chemistry of Contrast Agents in Medical Magnetic Resonance Imaging*; Wiley: London, 2001.
(4) Blasse, G. *J. Alloys Compd.* **1995**, *225*, 529.
(5) Hannah, S.; Lynch, V.; Guldi, D. M.; Gerasimchuk, N.; MacDonald, C. L. B.; Magda, D.; Sessler, J. L. *J. Am. Chem. Soc.* **2002**, *124*, 8416.

10.1021/ic0351996 CCC: $27.50
Published on Web 12/17/2003

weakly relaxed for trivalent lanthanide ions Ln^{III}, as a consequence of the shielding of the 4f orbitals by the filled $5s^25p^6$ subshells. These transitions are thus faint and keep their atomic nature; i.e., they appear as sharp lines, the energy of which is not much influenced by the surroundings of the metal ion, except for the crystal-field-induced fine structure. This apparent disadvantage may be turned into a serious asset since these lines are easily recognizable and useful for the development of versatile luminescent probes: the excited states have a long lifetime (micro- to milliseconds) and can be populated by the ligands via an energy-transfer process. Intense luminescence is accordingly generated in the visible and near-infrared with large apparent Stokes shifts,[6] and the Ln^{III} luminescence is easily separable from the background fluorescence, both spectrally and by time-resolved spectroscopy. Building on these significant advantages, lanthanide probes linked to monoclonal antibodies have been proposed for luminescent immunoassays displaying a better sensitivity than radioactive or biochemical assays.[7−9] The same methodology is adequate for probing protein−protein interactions and DNA hybridization.[10] Luminescent lanthanide chelates are also increasingly used as responsive analytical systems,[11] in color-tailored luminophores for simultaneous detection of multiple targets on DNA strands,[12] as labels for enhanced imaging of cancer,[13] and, generally speaking, in clinical applications and research.[14]

In this context, increasing the number of detectable probes on a single sample, for instance, by designing stains with tunable emission wavelengths and simultaneously tunable excited-state lifetimes, is potentially interesting.[12] With this in mind, we are developing synthetic strategies to produce 4f−4f heterobimetallic edifices because such molecular assemblies potentially combine two luminescent centers, or one magnetic center and one luminescent center, in a single probe. The recognition of one specific lanthanide ion in the presence of others is a difficult challenge in view of the limited differences in chemical properties and size of these ions (0.18 Å between La^{III} and Lu^{III} and ca. 0.015 Å between two consecutive ions). Basically, two strategies have been envisaged.

The first one simply relies on statistical formation of the heterobimetallic complex besides the homobimetallic ones from solutions containing a ditopic polydentate (usually symmetrical) ligand and a mixture of lanthanide ions. The first heterobimetallic 4f−4f complex structurally characterized, based on a decadentate Schiff base ligand, was obtained in this way and separated by selective crystallization.[15] In the past, we have resorted to this method, using either *p-tert*-butylcalix[8]arene[16] or a self-assembly process with ligand L^A (see Chart 1),[17] to study energy migration between two lanthanide ions lying at a known distance. Similar photophysical studies by other authors also relied on self-assembly processes with a symmetrical ligand.[18,19] Variations of this "statistical strategy" are the use of template reactions in the presence of two different lanthanide ions, leading to the formation of complexes with symmetrical compartmental and macrocyclic ligands,[20] and the addition of a second lanthanide ion to a solution of a mononuclear labile complex.[21]

Chart 1

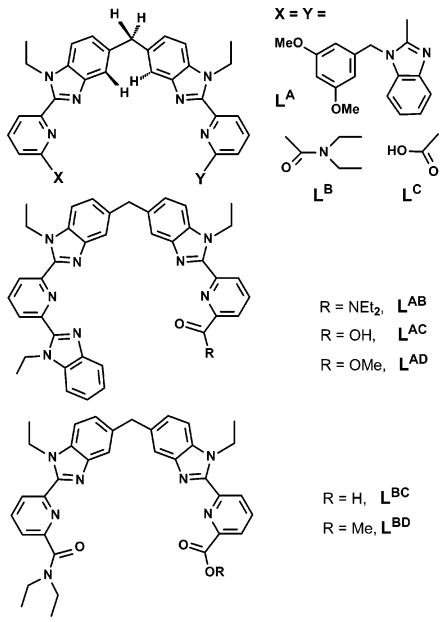

The second strategy utilizes guest molecules yielding sufficiently inert monometallic complexes to be reacted selectively with the second Ln^{III} ion. Triple-decker porphyrin and phthalocyanine complexes are obtained in this way.[22,23] Other smart receptors feature bis ligands such as two calix[4]arene[24] or cyclen[25] units linked by a separator. Our approach is similar to the first method, but takes advantage of self-assembly processes leading to the formation of coordination cavities specific to each ion. To achieve this, we have designed the unsymmetrical ligands L^{AB}, L^{AC}, and L^{BC}, derived from L^A,[17] L^B,[26] and L^C [27] (Chart 1), coded for

(6) Xiao Ming; Selvin, P. R. *J. Am. Chem. Soc.* **2001**, *123*, 7067.
(7) Hemmilä, I.; Mukkala, V. M. *Crit. Rev. Clin. Lab. Sci.* **2001**, *38*, 441.
(8) Hemmilä, I.; Ståhlberg, T.; Mottram, P. *Bioanalytical Applications of Labelling Technologies*; Wallac Oy: Turku, Finland, 1995.
(9) Mathis, G. In *Rare Earths*; Saez Puche, R., Caro, P., Eds.; Editorial Complutense: Madrid, 1998.
(10) Yam, V. W. W.; Lo, K. K. W. *Coord. Chem. Rev.* **1999**, *184*, 157.
(11) Parker, D. *Coord. Chem. Rev.* **2000**, *205*, 109.
(12) Chen, J. Y.; Selvin, P. R. *J. Am. Chem. Soc.* **2000**, *122*, 657.
(13) Bornhop, D. J.; Hubbard, D. S.; Houlne, M. P.; Adair, C.; Kiefer, G. E.; Pence, B. C.; Morgan, D. L. *Anal. Chem.* **1999**, *71*, 2607.
(14) Bünzli, J.-C. G. Metal Ions in Biological Systems. In *Metal Complexes in Tumor Diagnosis and as Anticancer Agents*; Sigel, A., Sigel, H., Eds.; Marcel Dekker Inc.: New York, 2003; Vol. 42, Chapter 2.
(15) Costes, J. P.; Dahan, F.; Dupuis, A.; Lagrave, S.; Laurent, J. P. *Inorg. Chem.* **1998**, *37*, 153.
(16) Bünzli, J.-C. G.; Froidevaux, P.; Harrowfield, J. M. *Inorg. Chem.* **1993**, *32*, 3306.
(17) Piguet, C.; Bünzli, J.-C. G.; Bernardinelli, G.; Hopfgartner, G.; Williams, A. F. *J. Am. Chem. Soc.* **1993**, *115*, 8197.
(18) Latva, M.; Makinen, P.; Kulmala, S.; Haapakka, K. *J. Chem. Soc., Faraday Trans.* **1996**, *92*, 3321.
(19) Lessmann, J. J.; Horrocks, W. d., Jr. *Inorg. Chem.* **2000**, *39*, 3114.
(20) Guerriero, P.; Vigato, P. A.; Bünzli, J.-C. G.; Moret, E. *J. Chem. Soc., Dalton Trans.* **1990**, 647.
(21) Hongye, S.; Chunhui, H.; Xianglin, J.; Guangxian, X. *Polyhedron* **1995**, *14*, 1201.
(22) Buchler, J. W.; De Cian, A.; Fischer, J.; Kihn-Botulinski, M.; Paulus, H.; Weiss, R. *J. Am. Chem. Soc.* **1986**, *108*, 3652.
(23) Ishikawa, N.; Iino, T.; Kaizu, Y. *J. Am. Chem. Soc.* **2002**, *124*, 11440.
(24) Wolbers, M. P. O.; Van Veggel, F. C. J. M.; Heeringa, R. H. M.; Hofstraat, J. W.; Geurts, F. A. J.; Vanhummel, G. J.; Harkema, S.; Reinhoudt, D. N. *Liebigs Ann.* **1997**, 2587.
(25) Jacques, V.; Desreux, J. F. *Top. Curr. Chem.* **2002**, *221*, 123.

the complexation of 4f ions. These ligands bear different end groups to generate, upon the self-assembly of three ligand strands around two metal centers, two cavities with sufficiently different properties to discriminate between lanthanide ions. In particular, L^{AB} generates an appreciable excess of HHH-heterobimetallic helicates (H stands for head) when the ionic radius difference between the two Ln^{III} ions is larger than 0.1 Å, as reported in a preliminary communication.[28] In this paper, we present the speciation of the lanthanide complexes formed in solution by L^{AB}, L^{AC}, and L^{BC} and the structural properties of the heterobimetallic helicates with L^{AB}, both in the solid state and in solution, and we discuss some thermodynamic aspects of the selective recognition process.

Experimental Section

Preparation of Ligands (Schemes 1 and 2). 3,3′-Dinitro-4,4′-bis(*N*-ethylamino)diphenylmethane (**2**),[29] 6-(*N*,*N*′-diethylcarbamoyl)pyridine-2-carboxylic acid (**3**),[30] 6-(1-ethylbenzimidazol-2-yl)pyridine-2-carboxylic acid (**5**),[27] and 6-(methoxycarbonyl)pyridine-2-carboxylic acid (**6**)[27] were prepared according to literature procedures. See the Supporting Information for detailed procedures and for the characterization of the other isolated compounds.

Preparation of the Complexes $[LnLn'(L^{AB})_3](ClO_4)_6$. The perchlorate salts $Ln(ClO_4)_3{\cdot}xH_2O$ (Ln = La−Lu, $x = 2-4$) were prepared from the corresponding oxides (Rhône-Poulenc, 99.99%) in the usual way.[31] *Caution! Perchlorate salts combined with organic ligands are potentially explosive and should be handled in small quantities and with adequate precautions.*[32] Heterobimetallic helicates were isolated with the lanthanide pairs LaEu, LaTb, LaEr, LaLu, PrEr, PrYb, and PrLu, as well as the homobimetallic complexes EuEu and TbTb. Synthetic procedures were similar to the one described below, with yields in the range 50−70%. Stock solutions of $Ln(ClO_4)_3{\cdot}xH_2O$ in CH_3CN were prepared by weighting. The water content of the salt and the concentration of the solutions were determined by complexometric titrations with $Na_2(H_2EDTA)$ in the presence of urotropine and xylene orange.[33] The lanthanide perchlorate solutions [$(3-4) \times 10^{-2}$ M, 1 equiv each] were added to 15.3 mg (21.8 μmol, 3 equiv) of L^{AB} in 150−200 μL of CH_3CN, and the resulting solution was stirred at room temperature for 90 min. Diethyl ether was then slowly diffused, inducing the formation of crystalline needles. For LaEu, LaTb, PrEr, PrLu, and EuEu, dissolution of ca. 10 mg of complex in 0.8 mL of CH_3CN/C_2H_5CN (1:1) followed by slow diffusion of ^{t}BuOMe for 8−10 days yielded X-ray-quality prismatic crystals. The complexes were characterized by IR and elemental analyses (Supporting Information). Samples of LnLu and Ln_2 (Ln = La, Ce, Pr, Nd, Sm, Eu, Lu) complexes with L^{AB} for NMR measurements were prepared in a similar fashion, except that, after being stirred for 90 min, the solutions were evaporated to dryness. The residues were dried in a vacuum overnight, redissolved in 0.6 mL of CD_3CN, and transferred to NMR tubes.

Spectroscopic Measurements. UV−vis spectra were measured with Perkin-Elmer Lambda 7 and Lambda 900 spectrometers using 0.1 or 1 cm quartz cells. Reflectance spectra were recorded as finely ground powders dispersed in MgO (5%) with MgO as the reference with a Perkin-Elmer Labsphere SRS-99-010-9976-A integrating sphere. IR spectra were obtained from KBr pellets with a Mattson α-Centauri FT-IR spectrometer. ESI-MS spectra used for the characterization of organic compounds were recorded in MeOH or CH_3CN with a Finnigan SSQ-710C spectrometer. ESI-MS spectra were measured in the pneumatically assisted mode from 10^{-3} to 10^{-4} M acetonitrile solutions on an API III tandem spectrometer (PE Sciex) and an LCQ ion trap (Thermo Finnigan) by infusion at 4−10 mL/min. The spectra were recorded under low up-front declustering or collision-induced dissociation (CID). 1D ^{1}H NMR spectroscopy as well as 2D COSY and ROESY experiments were performed on Bruker AM 360 (360 MHz) and DRX 400 and Avance 400 (400 MHz) spectrometers. The experimental procedures for high-resolution, laser-excited luminescence studies have been published previously.[34] Quantum yields were determined with respect to quinine sulfate, as previously described,[35] from ca. 1.5×10^{-4} M solutions to avoid decomplexation, but at wavelengths where (i) the Lambert−Beer law is obeyed and (ii) the absorption of the reference closely matches that of the sample. Ligand excitation and emission spectra were recorded on a Perkin-Elmer LS-50B spectrometer equipped for low-temperature (77 K) measurements.

X-ray Crystal Structure Determinations. Data were collected at 143 K on a marresearch mar345 IPDS image-plate diffractometer (Supporting Information). Data reduction was carried out with CrysAlis RED, release 1.7.0.[36] An empirical absorption correction was applied to LaTb and EuEu (program DELABS).[37] Structure solution and refinement as well as molecular graphics and geometrical calculations were performed for all structures with the SHELXTL software package, release 5.1.[38] The structures were refined using the full-matrix-block least-squares method on F^2 with fixed anisotropic displacement parameters. H atoms were placed in calculated positions using the "riding model". In the case of compounds PrEr and PrLu, and in view of the relatively poor data, all atoms except the two metals were retained as isotropic and no hydrogen atoms were introduced. Some disorder problems deal with two ethyl groups (N6, C40, C41; N18, C85, C86) and with the solvent molecules (retained as isotropic). To obtain reasonable parameters for such moieties, cards DFIX and DELU were employed. The structure of LaEu is already deposited with the CCDC database (Reference No. 172173).

Results

Ligand Design, Synthesis, and Properties. The ligand design is based on the following considerations. In preceding works, we have shown that the aromatic tridentate ligands L^i ($i = 1-3$; see Chart 2) react with Ln^{III} ions to yield stable triple helical complexes $[Ln(L^i)_3]^{3+}$ in acetonitrile;[39−41] in addition, the analogous dipicolinate complexes [Ln(L^4-

(26) Martin, N.; Bünzli, J.-C. G.; McKee, V.; Piguet, C.; Hopfgartner, G. *Inorg. Chem.* **1998**, *37*, 577.
(27) Elhabiri, M.; Scopelliti, R.; Bünzli, J.-C. G.; Piguet, C. *J. Am. Chem. Soc.* **1999**, *121*, 10747.
(28) André, N.; Scopelliti, R.; Hopfgartner, G.; Piguet, C.; Bünzli, J.-C. G. *Chem. Commun.* **2002**, 214.
(29) Piguet, C.; Bernardinelli, G.; Bocquet, B.; Quattropani, A.; Williams, A. F. *J. Am. Chem. Soc.* **1992**, *114*, 7440.
(30) Piguet, C.; Bünzli, J.-C. G.; Bernardinelli, G.; Hopfgartner, G.; Petoud, S.; Schaad, O. *J. Am. Chem. Soc.* **1996**, *118*, 6681.
(31) Desreux, J. F. In *Lanthanide Probes in Life, Chemical and Earth Sciences. Theory and Practice*; Bünzli, J.-C. G., Choppin, G. R., Eds.; Elsevier Science B.V.: Amsterdam, 1989; Chapter 2.
(32) Raymond, K. N. *Chem. Eng. News* **1983**, *61*, 4.
(33) Schwarzenbach, G. *Complexometric Titrations*; Chapman & Hall: London, 1957.
(34) Rodriguez-Cortinas, R.; Avecilla, F.; Platas-Iglesias, C.; Imbert, D.; Bünzli, J.-C. G.; de Blas, A.; Rodriguez-Blas, T. *Inorg. Chem.* **2002**, *41*, 5336.
(35) Zucchi, G.; Ferrand, A.-C.; Scopelliti, R.; Bünzli, J.-C. G. *Inorg. Chem.* **2002**, *41*, 2459.
(36) Oxford Diffraction Ltd., Abingdon, Oxfordshire, U.K., 2003.
(37) Walker, N.; Stuart, D. *Acta Crystallogr.* **1983**, *A39*, 158.
(38) SHELXTL, Bruker AXS Inc., Madison, WI 53719, 1997.

Chart 2

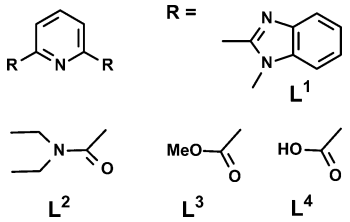

$2H)_3]^{3-}$ are well-known.[42] Ligands L^{2-4} produce a commonly observed trend in the stability of lanthanide complexes: log β_{13} increases with increasing atomic number, the Lu^{III} complexes being 50−340-fold more stable than the La^{III} compounds.[40−42] On the other hand, L^1 induces a peculiar behavior. From La^{III} to Gd^{III}, the stability increases slightly by a factor of 6 and then decreases sharply, the Lu^{III} complex being 8000-fold less stable than the Gd^{III} one. This size-discriminating effect has been interpreted as arising from the difficulty for the ligand strands to wrap tightly around the smaller lanthanide ions.[39] Less systematic data are available for the symmetrical ditopic ligands L^A, L^B, and L^C, but the stability constants with the bis(benzimidazole)-pyridine derivative L^A show the Lu^{III} bimetallic helicate being 2.5−4.5 orders of magnitude less stable in acetonitrile than the corresponding complexes with La^{III} and Eu^{III}.[17] Moreover, $[Ln_2(L^B)_3]^{6+}$ helicates (Ln = La, Eu) are 2−3 orders of magnitude more stable than $[Ln_2(L^A)_3]^{6+}$, while $[Eu_2(L^C-2H)_3]$ is extremely stable in water, with a cumulative log β_{23} in the range 51−52.[27,43] It was therefore logically expected that unsymmetrical ditopic ligands combining L^1 with either L^2 or L^4 (L^{AB}, L^{AC}) would allow the simultaneous recognition of two Ln^{III} ions differing in size. Ligand L^{BC} was mainly synthesized for comparison reasons, while ligands L^{AD} and L^{BD} were obtained as reaction intermediates but were not tested since ester groups are not good complexing moieties for lanthanide ions.[41,44] The synthetic procedure is based on the symmetrical dinitro compound **2** (Schemes 1 and 2), which is successively N-substituted by the corresponding end groups. The strategy adopted involves several common intermediates to minimize the large synthetic effort required by unsymmetrical compounds. Ligands L^{AB}, L^{AC}, and L^{BC} were obtained in reasonably good yields from intermediates **7a**, **7b**, and **9**, respectively, by a modified[26] double Phillips coupling reaction to form the benzimidazole units.

In $CDCl_3$, the three ditopic ligands adopt the usual *trans* conformation,[17,26,27] as ascertained by ^1H NMR COSY and ROESY experiments. The spatial interactions, which are the same for all three ligands, are shown for L^{AB} in Figure 1,

Scheme 1 [a]

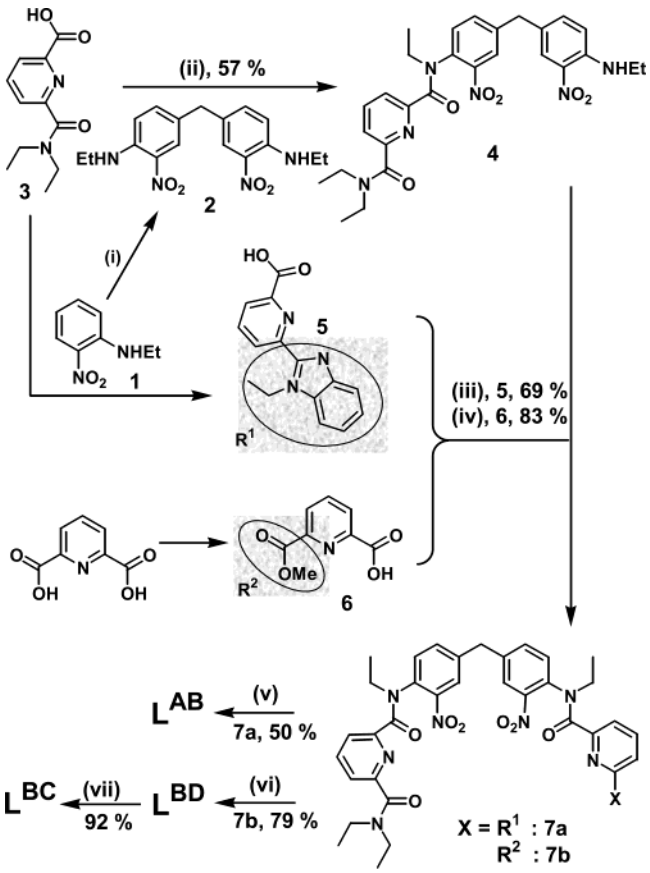

[a] Reagents and conditions: (i) $(CH_2O)_n$, HCl (37%); (ii) **3** + $SOCl_2$, CH_2Cl_2, DMF; **2**; (iii) **5** + $SOCl_2$, CH_2Cl_2, DMF; (iv) **6** + $SOCl_2$, CH_2Cl_2, DMF; (v) Fe, HCl, EtOH, H_2O; (vi) Fe, HCl, EtOH, H_2O; (vii) KOH (1 M), EtOH, H_2O.

Scheme 2 [a]

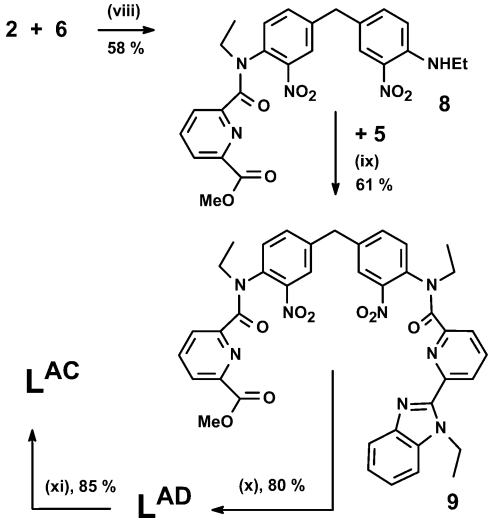

[a] Reagents and conditions: (viii) **6** + $(COCl)_2$, toluene, DMF; **2**; (ix) **5** + $(COCl)_2$, toluene, DMF; (x) Fe, HCl, EtOH, H_2O; H_2SO_4 (96%), MeOH; (xi) KOH (1 M).

along with an optimized structure from molecular mechanics calculations. The absence of NOE effects between H1 and the NEt_2 groups, H3 and H4, H13 and H15, and H17 and H18, for instance, is in line with N-donor atoms of the pyridyl groups being in the *trans* configuration with respect to the O and/or N donor atoms of the 2,6-substituents. Complex-

(39) Petoud, S.; Bünzli, J.-C. G.; Renaud, F.; Piguet, C.; Schenk, K. J.; Hopfgartner, G. *Inorg. Chem.* **1997**, *36*, 5750.
(40) Renaud, F.; Piguet, C.; Bernardinelli, G.; Bünzli, J.-C. G.; Hopfgartner, G. *Chem. Eur. J.* **1997**, *3*, 1646.
(41) Renaud, F.; Piguet, C.; Bernardinelli, G.; Bünzli, J.-C. G.; Hopfgartner, G. *Chem. Eur. J.* **1997**, *3*, 1660.
(42) Grenthe, I. *J. Am. Chem. Soc.* **1961**, *83*, 360.
(43) Elhabiri, M.; Hamacek; Bünzli, J.-C. G.; Albrecht-Gary, A.-M. *Eur. J. Inorg. Chem.* **2003**, in press, DOI 10.1002/ejic.200300549.
(44) Thompson, L. C. In *Handbook on the Physics and Chemistry of Rare Earths*; Gschneidner, K. A., Jr., Eyring, L., Eds.; North-Holland: Amsterdam, 1979; Vol. 3, Chapter 25.

Table 1. Selected Species Observed by ESI-MS in Acetonitrile Solutions with 2:3 Ln:L or 1:1:3 Ln:Ln′:L Stoichiometry (L = L^{AB} and $(L^{AC}\text{-}H)^-$; $[Ln]_t = 10^{-3}$ M)

species	*m/z* obsd	*m/z* calcd	species	*m/z* obsd	*m/z* calcd
$[La_2(L^{AB})_3]^{6+}$	397.3	397.2	$[La_2(L^{AB})_3(ClO_4)_3]^{3+}$	894.3	894.3
$[LaEu(L^{AB})_3]^{6+}$	399.6	399.4	$[LaEu(L^{AB})_3(ClO_4)_3]^{3+}$	898.3	898.1
$[Eu_2(L^{AB})_3]^{6+}$	401.8	401.6	$[Eu_2(L^{AB})_3(ClO_4)_3]^{3+}$	902.6	902.6
$[La_2(L^{AB})_3(ClO_4)]^{5+}$	496.4	496.6	$[La_2(L^{AC}\text{-}H)_3]^{3+}$	738.2	738.3
$[LaEu(L^{AB})_3(ClO_4)]^{5+}$	499.0	499.2	$[LaEu(L^{AC}\text{-}H)_3]^{3+}$	742.7	742.7
$[Eu_2(L^{AB})_3(ClO_4)]^{5+}$	501.8	501.8	$[Eu_2(L^{AC}\text{-}H)_3]^{3+}$	747.3	747.0
$[La_2(L^{AB})_3(ClO_4)_2]^{4+}$	645.7	645.6	$[La_2(L^{AC}\text{-}H)_3(ClO_4)]^{2+}$	1157.1	1157.2
$[LaEu(L^{AB})_3(ClO_4)_2]^{4+}$	648.8	648.8	$[LaEu(L^{AC}\text{-}H)_3(ClO_4)]^{2+}$	1163.6	1163.8
$[Eu_2(L^{AB})_3(ClO_4)_2]^{4+}$	652.2	652.1	$[Eu_2(L^{AC}\text{-}H)_3(ClO_4)]^{2+}$	1170.6	1170.3

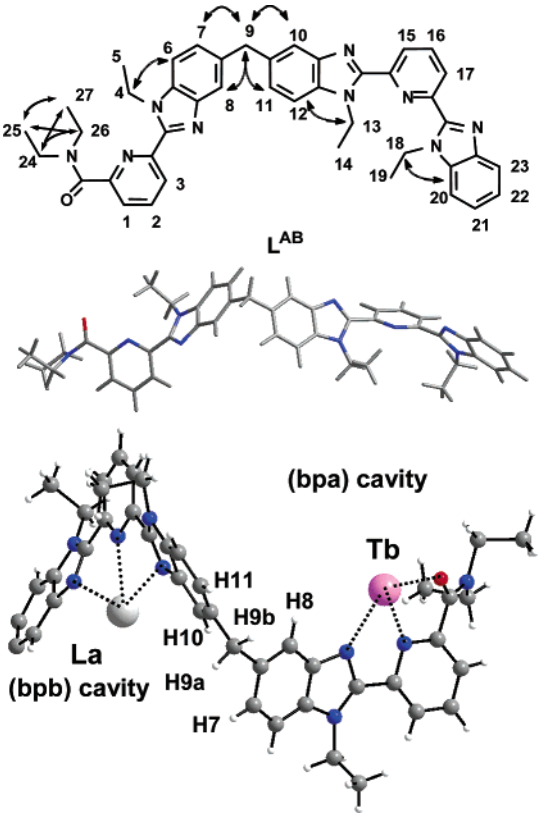

Figure 1. Spatial interactions evidenced in L^{AB} by ^{1}H NMR (top), structure optimized by MM2 molecular mechanics calculations (middle), and conformation of the coordinated ligand with H atoms between which NOE effects are observed (bottom).

ation to Ln^{III} ions therefore requires a conformational work to rotate the two ends of the ditopic ligands so that the three donor atoms of each coordinating unit are adequately positioned.

Interaction between L^{AB} and Ln^{III} Ions: Speciation in Acetonitrile. ESI-MS spectra of stoichiometric 2:3 mixtures of one lanthanide perchlorate (10^{-3} M) and L^{AB} in acetonitrile clearly evidence the main presence of the homobimetallic helicate, as characterized by its perchorate adducts $[Ln_2(ClO_4)_xL_3]^{6+}$ (Ln = La, Eu; L = L^{AB}; $x = 0-3$; see Table 1). Titration of L^{AB} (1.6×10^{-4} M) with $Eu(ClO_4)_3 \cdot 4.5H_2O$ (8.9×10^{-3} M) in dried acetonitrile monitored by UV−vis spectrophotometry confirmed this finding. A single break was observed in the absorbance versus $R = [Ln]_t/[L^{AB}]_t$ plots at $R = 0.67$, and factor analysis pointed to only two absorbing species for ratios in the range $R = 0-2$. Data could be satisfactorily fitted to eq 1 with $\log \beta_{23} = 23.9 \pm 0.5$, as compared to ~22 for $[Eu_2(L^A)_3]^{6+}$ [17] and 24 ± 1 for $[Eu_2(L^B)_3]^{6+}$.[26]

$$2Eu^{3+} + 3L^{AB} \leftrightarrows [Eu_2(L^{AB})_3]^{6+} \ (\log \beta_{23}) \qquad (1)$$

This study has been completed by an ^{1}H NMR investigation of the La^{III} and Lu^{III} systems for $R = 0.3-1.0$. With L^{AB} in acetonitrile-d_3, two species were observed for La^{III}, for R ratios in the range 0.3−0.67, while a third, minor one, was detected for $R = 1$. Analysis of the number of observed signals (Table 2) allowed us to assign the major species to the HHH and HHT helicates (T stands for tail), whereas the minor species most probably corresponds to a 2:2 species which was also detected in the ESI-MS spectrum for $R = 1$. Kinetic investigations have shown the 2:2 species being a key intermediate in the formation of the bimetallic helicates with L^A [45] and $(L^C\text{-}H)^-$.[43] The relative proportions of the two major species were estimated on the basis of signal integration. For $R = 0.67$, they substantially deviate from the statistical distribution (25% HHH, 75% HHT), which points to a clear stabilization of the HHH species: 72% for La^{III} and ca. 65% for Lu^{III}. In the latter case, other species are seen, 1:1, 2:2, 1:2, and possibly 1:3, indicating a less stable bimetallic helicate compared to that of La^{III}, a trend expected from the smaller affinity of the benzimidazoyl group for the smaller Ln^{III} ions.[39]

As for the systems containing one type of Ln^{III} ion, we have probed by ESI-MS the nature of the species present in solutions containing L^{AB} and two different Ln^{III} perchlorates in equimolar proportion (total concentration 10^{-3} M). The spectra evidence the prominent formation of bimetallic species which were identified by their adduct formation with perchlorate (Table 1) as well as by the isotopic distribution, one example of which is given in Figure 2. In addition, minor peaks have been observed which could be assigned to 1:1, 1:2, and 2:2 Ln:L species. The intensity of these species increases when the Ln:Ln′:L ratio is lowered to 1:1:2, clearly evidencing the presence of the kinetically important 2:2 species.[45] Replacing the perchlorate counterions by triflate moieties modifies considerably the speciation; in particular, the signals assigned to the 2:3 helicates lose intensity to the benefit of the 2:2 (respectively 1:1:2) species, as was observed for the symmetrical ligand L^B.[26] For each pair of lanthanide ions analyzed, the relative concentrations of the

(45) Hamacek; Blanc, S.; Elhabiri, M.; Leize, E.; Van Dorsselaer, A.; Piguet, C.; Albrecht-Gary, A.-M. *J. Am. Chem. Soc.* **2003**, *125*, 1541.

Table 2. Observed and Theoretical Number of ^{1}H NMR Signals Expected for HHH-$[La_2(L^{AB})_3]^{6+}$ and HHT-$[La_2(L^{AB})_3]^{6+}$ [a,b]

protons 5, 14, 19, 25, and 27			protons 4, 13, 18, 24, and 26		protons 9a and 9b		protons 8 and 10		others	
	obsd	theor	obsd	theor	obsd	theor	obsd	theor	obsd	theor
HHH	5 t	5 t	10 dq	10 dq	2 d	2 d	2 s	2 s	14	14
HHT	12 t[c]	15 t	12 dq[c]	30 dq	2 d	6 d	6 s	6 s	22[c]	42

[a] For proton numbering, see Figure 1. [b] Key: s, singlet; d, doublet; t, triplet; dq, doublet of quadruplets. [c] Overlapping signals.

Table 3. Percentages of Homo- and Heterobimetallic Triple-Stranded Helicates in Acetonitrile with Respect to the Total Amount of Helicates, As Determined by ESI-MS and NMR in Stoichiometric Solutions Ln:Ln′:L = 1:1:3

L	LnLn′	% LnLn	% Ln′Ln′	% LnLn′	% LnLn′ [a]	$\Delta(\Delta G)^c$/ kJ·mol^{-1}	L	LnLn′	% LnLn	% Ln′Ln′	% LnLn′
L^{AB}	LaLu	5	6	89	90	−10.4	L^{AC}	LaEr	27	11	62
	EuLu	25	18	57	65	−1.5		LaEu	23	28	49
	LaYb	b	b	b	87	−9.4		LaLu	21	0	79
	LaEr	12	9	79	81	−6.6		PrLu	33	4	63
	PrEr	18	12	70	b	−4.3		EuTb	24	27	49
	EuEr	22	23	55	b	−1.0		EuLu	47	0	53
	EuTb	22	27	51	b	−0.3		ErLu	30	20	50
	LaEu	20	15	65	b	−3.1	L^{BC}	LaLu	51	18	31

[a] Determined by ^{1}H NMR. [b] Not measured. [c] See the text and eq 16.

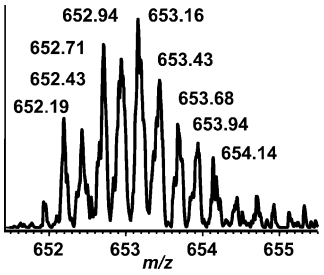

Figure 2. Isotopically resolved ESI-MS spectra of $\{[PrEr(L^{AB})_3](ClO_4)_2\}^{4+}$ aquired at *m*/*z* 653.16 Th (zoom scan mode).

homo- and heterobimetallic helicates have been estimated from the intensities of the peaks generated by the mono- and diperchlorato adducts (Supporting Information). It is indeed expected that solvation effects will be the same for a series of related species having the same total charge. Data reported in Table 3 display appreciable deviations from a statistical distribution considering the two ligand cavities as equivalent: 25% of each homobimetallic species and 50% of the heterobimetallic helicate. There is a marked preference for the heterobimetallic helicate, which increases with increasing difference in atomic numbers.

^{1}H NMR spectra give more insight into the speciation since they allow HHH and HHT isomers to be distinguished, but the potential presence of these two isomers for both homo- and heterobimetallic helicates leads sometimes to rather complex spectra. However, the NMR spectrum of a stoichiometric solution, La:Lu:3L^{AB} (Figure 3), results in a clear interpretation, consistent with the ESI-MS data. Most of the signals can be interpreted as arising from the HHH-heterobimetallic species (90%), with three equivalent ligand strands. In particular, protons H8 and H10 generate singlets at high field, which is characteristic of the helical wrapping of the ligands, these protons lying in the shielding cone of the benzimidazole moieties borne by the two other ligand strands. The five methylene groups of the ethyl substituents are diastereotopic and produce 10 doublets of quadruplets (appearing as pseudosextets), pointing to the absence of P ↔ M interconversion on the NMR time scale. This is in line

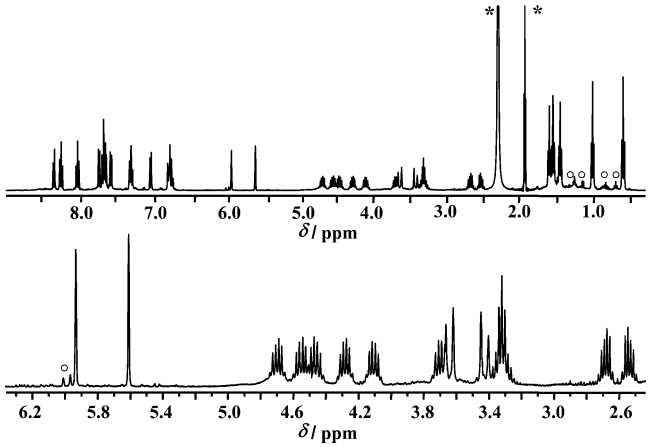

Figure 3. ^{1}H NMR spectrum of a 10^{-2} M solution of $[LaLu(L^{AB})_3](ClO_4)_6 \cdot 3H_2O$ in CD_3CN. Asterisks denote H_2O and CHD_2CN, and open circles signals from homobimetallic species.

with the two protons of the methylene bridge being diastereotopic and appearing as two doublets at 3.4 and 3.6 ppm with a ^2J coupling constant equal to 17.8 Hz. Assignment of the ^{1}H NMR signals of HHH-LaLu (Supporting Information) is confirmed by 2D NMR experiments (COSY, ROESY). NOE effects between H1 and H24, H3 and H4, H13 and H15, and H17 and H18, which are not seen in the free ligand, are consistent with a *cis*−*cis* conformation typical of the coordinated ligand strand. Moreover, the helical conformation of the ligand strands (see Figure 1) is reflected in NOE effects being observed between H7 and H9a and H9b and H11, while very weak interligand interactions between H4 and H11, H7 and H13, H7 and H14, and H13 and H18 reflect the close spatial proximity of the three ligand strands. Finally, the chemical shifts of the protons located on the benzimididazole−pyridine−carboxamide (bpa) end of the ligand are quite similar to those of the HHH-Lu_2 complex ($\Delta\delta$ typically ∼0.02 ppm), and the same correspondence holds between the chemical shifts of the protons on the benzimidazole−pyridine−benzimidazole (bpb) end of the ligand and those of the HHH-La_2 complex. As an example, the match between the signals of protons H1, H2,

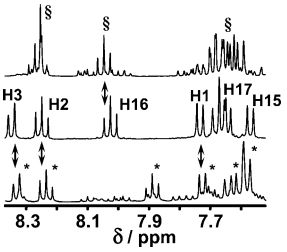

Figure 4. Part of the aromatic region of the ^{1}H NMR spectra of HHH-$[La_2(L^{AB})_3]^{6+}$ (top, §), HHH-$[LaLu(L^{AB})_3]^{6+}$ (middle), and HHH-$[Lu_2(L^{AB})_3]^{6+}$ (bottom, *), 10^{-2} M in acetonitrile, at room temperature. Corresponding protons are indicated with double arrows.

and H3 in HHH-LaLu and those in HHH-Lu_2 is illustrated in Figure 4, while further examples are given in the Supporting Information. These data suggest that the ligand is coordinated to the smaller Lu ion by the bpa end and to the larger La ion by the bpb compartment. Integration of the signals arising from hetero- and homobimetallic species leads to proportions of these species comparable with the ones determined by ESI-MS (Table 3), despite the concentration difference.

Crystal Structures of the Homo- and Heterobimetallic Helicates with L^{AB}. By working under stoichiometric conditions, single crystals of reasonable X-ray quality could be obtained upon diffusion of diethylether into a mixture of acetonitrile and propionitrile for four heterobimetallic helicates and one homobimetallic helicate, LaEu, LaTb, PrEr, PrLu, and EuEu (Supporting Information). The single crystals of LaEu are of the best quality, and the refinement could be carried out with most atoms considered as being anisotropic, except those of the solvation molecules and of the ethyl substituents, which are disordered. On the other hand, relatively poor crystals could only be grown for the other compounds, and their structures are essentially presented to prove the isostructurality of the series and to discuss the coordination polyhedra, as well as the metal−metal distances. The atom-numbering scheme is the same for the five helicates and is partly shown for LaTb in Figure 5. The crystal structures are comprised of isolated $[LnLn'(L^{AB})_3]^{6+}$ cations. All the helicates display the same HHH ligand arrangement with, for the heterobimetallic complexes, the bpa groups bound to the heavier Ln^{III} ion, while the bpb ends of the ligands building a coordination cavity for the lighter Ln^{III} ion. For the heterobimetallic helicates, the assignment of the metal ions to each coordinating site, bpb and bpa, has been tested by using two different models: (I) Ln(bpb)−Ln′(bpa) and (II) Ln(bpa)−Ln′(bpb), where Ln stands for the lighter Ln^{III} ion and Ln′ for the heavier one. In each case, the smallest R1 factor was obtained for the Ln(bpb)−Ln′(bpa) model (Supporting Information). A third model (III) taking into account mixtures of homobimetallic helicates x(LnLn) + (1 − x)Ln′Ln′ with variable populations x was also tried and converged for x between 0.47 and 0.49 with R1 factors close to the ones generated by model I. However, an exact comparison could not be carried out, the data being of insufficient quality to allow solving the structures with strictly the same parameters as in the previous two models. A better hint to the $[LnLn'(L^{AB})_3]^{6+}$ entities

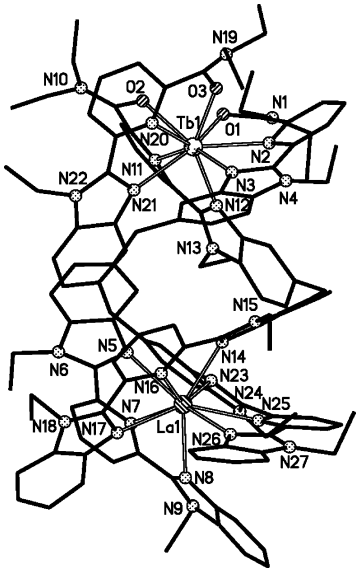

Figure 5. Partial atom-numbering scheme in the molecular structure of $[LaTb(L^{AB})_3](ClO_4)_6\cdot 3MeCN\cdot 3EtCN$.

being essentially heterobimetallic is given by the metal−donor atom distances reported in Table 4 for LaEu and in the Supporting Information for the other helicates. Comparisons between these distances and the distances found in the homobimetallic helicates with L^A (EuEu) and L^B (TbTb), with the homotrimetallic helicate with L^{BAB} (EuEuEu; see Chart 3), and with the heterobimetallic 4f−3d helicates with L^{Ba} (LaFe, LaCo, EuZn, LuCr) and L^{Bb} (EuZn) are shown in Figure 6. Complexes with the same cation in the same coordination site have identical Ln−X distances: see for instance Tb^{III} in the bpa site of $[LaTb(L^{AB})_3]^{6+}$ and $[Tb_2(L^B)_3]^{6+}$,[26] or Eu^{III} in the bpa site of $[LaEu(L^{AB})_3]^{6+}$ compared with $[EuZn(L)_3]^{5+}$ (L = L^{Ba}, L^{Bb})[30,46] or $[Eu_3(L^{BAB})_3]^{9+}$,[47] which confirms our assignment for LaEu and LaTb. In the other heterobimetallic helicates with L^{AB}, the bpa site is always associated with Ln−L distances shorter than those reported in the literature for $[LaCo(L^{Ba})_3]^{6+}$,[48] $[EuZn(L)_3]^{5+}$ (L = L^{Ba}, L^{Bb}),[30,46] or $[Eu_3(L^{BAB})_3]^{9+}$,[47] which means that this site is mainly occupied by the smaller lanthanide ion, Er or Lu. As a result, Ln−X distances in the bpb site are longer than in $[Eu_2(L^A)_3]^{6+}$, in line with the presence of the larger cation in this site (Pr, La). On a whole, however, these data do not allow us to rule out that the crystals incorporate small amounts of species other than the HHH-heterodimetallic helicates, either HHT helicates or homobimetallic complexes. This probably explains the poorer quality of some of the crystals.

The ligand strands are wrapped around a pseudo-C_3 axis going through the two metal ions. Perchlorate anions and solvent molecules lie outside the first coordination sphere of the metal ions. Very weak interstrand interactions are

(46) Edder, C.; Piguet, C.; Bernardinelli, G.; Mareda, J.; Bochet, C. G.; Bünzli, J.-C. G.; Hopfgartner, G. *Inorg. Chem.* **2000**, *39*, 5059.
(47) Floquet, S.; Ouali, N.; Bocquet, B.; Bernardinelli, G.; Imbert, D.; Bünzli, J.-C. G.; Hopfgartner, G.; Piguet, C. *Chem. Eur. J.* **2003**, *9*, 1860.
(48) Rigault, S.; Piguet, C.; Bernardinelli, G.; Hopfgartner, G.; *Angew. Chem., Int. Ed.* **1998**, *37*, 169.

Table 4. Ln^{III}-Donor Atom Distances in $[LaEu(L^{AB})_3](ClO_4)_6 \cdot 3MeCN \cdot 3EtCN$[a]

Ln	Ln-O/Å		Ln-N(py)/Å		Ln-N(imid)/Å	
Eu	O1	2.416(5)	N2	2.632(7)	N3	2.585(8)
	O2	2.385(7)	N11	2.625(8)	N12	2.570(6)
	O3	2.390(6)	N20	2.608(6)	N21	2.600(7)
	mean	2.40(2)	mean	2.62(1)	mean	2.59(2)
Ln	Ln-N(imid)$_t$/Å		Ln-N(py)/Å		Ln-N(imid)$_b$/Å	
La	N8	2.637(7)	N7	2.626(7)	N5	2.630(7)
	N17	2.682(7)	N16	2.667(6)	N14	2.621(7)
	N26	2.649(8)	N25	2.670(7)	N23	2.673(7)
	mean	2.66(2)	mean	2.65(2)	mean	2.64(3)

[a] For the atom-numbering scheme, see Figure 5; (imid)$_t$ = terminal imidazole; (imid)$_b$ = bridging imidazole.

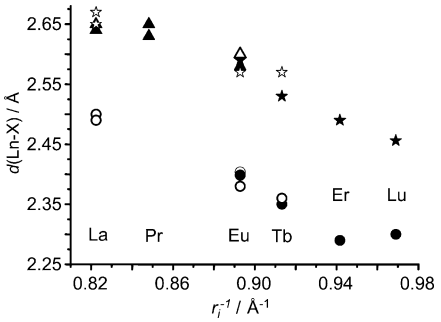

Figure 6. Mean Ln−X distances (Å) in various helicates versus the inverse ionic radius for a coordination number of 9: solid symbols, $[LnLn'(L^{AB})_3]^{6+}$; open symbols, reference compounds (see the text); triangles, Ln−N(py) of the bpb site; stars, Ln−N(benzimide) of the bpa site; circles, Ln−O(amide).

Chart 3

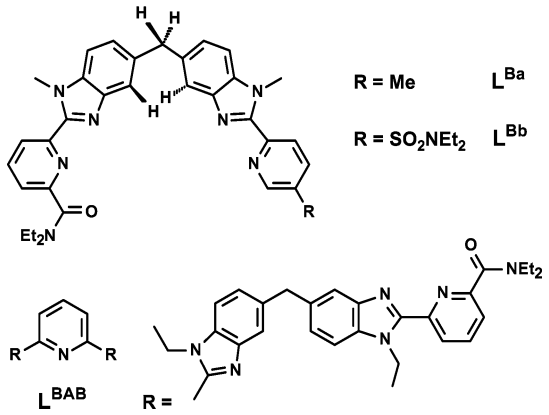

detected between imidazole groups located at the bpb end of the ligands: interplanar distances are around 4 Å, compared to 3.7 Å in $[Eu_2(L^A)_3]^{6+}$ and 3.9 Å in $[Eu_2(L^B)_3]^{6+}$.

The coordination polyhedra are slightly distorted tricapped trigonal prisms with coordination number 9 and in which the upper tripods are defined by the three amide O atoms for the heavier Ln^{III} ion and by the three N atoms from the nonbridging benzimidazole units for the lighter Ln^{III} ion. The molecular pseudo-C_3 axis goes through the middle of the upper and lower triangles. A more quantitative analysis has been performed according to the previously published procedure (Supporting Information).[27] In the case of LaEu, the two faces of the prism are parallel (dihedral angle $\alpha = 0.4°$), but cannot be superimposed, due to the constraints generated by the ligand strands (the rotation angle ω_i amounts to 11.1°). The Eu^{III} ion lies 0.175 Å under the capping plane

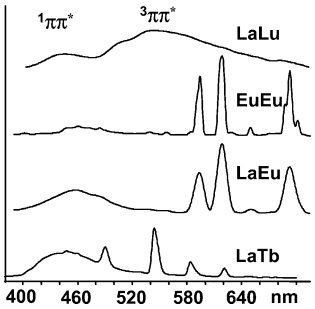

Figure 7. Emission spectra (fluorescence mode) of $[LnLn'(L^{AB})_3](ClO_4)_6 \cdot xH_2O$ in the solid state, at 77 K, upon ligand excitation (ca. 29350 cm^{-1}). Vertical scale: arbitrary units.

formed by the three N atoms from the pyridine moieties, and the deviations of the Eu−X (X = O, N) distances with respect to the mean values are smaller than 1.3%, indicating a fairly regular polyhedron, comparable to the one found for $[Tb_2(L^B)_3]^{6+}$.[26] The geometry of the La^{III} coordination polyhedron is comparable, with $\alpha = 2.5°$, $\omega_i = 15.9°$, and La−X deviations from the mean values amounting to at most 1.2%; on the other hand, the other angles characterizing the coordination polyhedron display a larger spread with respect to their mean values, pointing to a slightly more distorted arrangement. Similar considerations hold for the other helicates, but when the cation size decreases, the upper and lower faces of the coordination polyhedra become more eclipsed and the prism becomes more compressed.

Luminescent Properties of the $[LnLn'(L^{AB})_3](ClO_4)_6 \cdot xH_2O$ Helicates. At room temperature, ligand excitation of LaLu results in a broad-band, ligand-centered $^1\pi\pi^*$ emission with a maximum at 22570 cm^{-1} which is blue shifted at 77 K (23090 cm^{-1}) and which almost disappears upon enforcing a short time delay. At low temperature, a second, structured band comes out, assigned to emission from a $^3\pi\pi^*$ state, which extends to about 14300 cm^{-1}, with a maximum at 18620 cm^{-1} and a 0−0 transition at 20000 cm^{-1} (Figure 7, Supporting Information). This emission is characterized by a double-exponential decay with lifetimes τ of 7 ± 1 and 70 ± 5 ms, consistent with the existence of two triplet states located each on one compartment (bpa, bpb) of the ligand. As a comparison, the energy of the $^3\pi\pi^*$ 0−0 transition in the homobimetallic helicates $[La_2(L^A)_3]^{6+}$ and $[Lu_2(L^B)_3]^{6+}$ was found to be 20920 and 20200 cm^{-1}, respectively, while τ was equal to 108 ± 5 and 90 ± 5 ms, respectively. The fluorescence quantum yield, determined on 1.5 × 10^{-4} M

solutions in acetonitrile, is also relatively small: 7.3% and 8.5% for the LaLa and LaLu helicates, respectively.

Emission spectra of the homobimetallic (EuEu) and heterobimetallic (LaEu, LaTb) helicates containing a luminescent Ln^{III} ion still display some signal from the ligand $^1\pi\pi^*$ emission, the quantum yield of which drops from 8.5% for LaLu to 2.3% for LaEu and 6% for EuEu. Very weak emission from the ligand $^3\pi\pi^*$ is also seen in the LaEu spectrum (Figure 7). This points to a relatively poor sensitization of the Ln^{III} ions: the quantum yield of the metal-centered luminescence upon ligand excitation (29500−30000 cm^{-1}) amounts to $Q^{Eu}_L = 1.9\%$ for LaEu and 0.6% for EuEu. On the other hand, lifetimes of the excited Eu($^5D_0$) state are large, 2.20 ± 0.01 (LaEu) and 2.26 ± 0.05 (EuEu) ms at 77 K, and do not depend much upon the temperature (1.87 ± 0.01 and 1.79 ± 0.03 ms at 295 K, respectively), consistent with water being absent from the inner coordination sphere. The LaTb luminescence is very weak at room temperature, preventing the determination of the quantum yield of the metal-centered emission, due to a back-transfer process: τ decreases from 0.91 ± 0.04 ms at 77 K to less than 0.06 ms at room temperature. This is understandable because the Tb($^5D_4$) level lies about 500 cm^{-1} above the energy of the 0−0 component of the triplet state, while Eu($^5D_0$) is located 2750 cm^{-1} below. Altogether, the emerging picture is that most of the deexcitation goes through nonradiative paths and that L^{AB} is a modest sensitizer of the Eu^{III} luminescence, much better than L^A ($Q^{Eu}_L \approx 0.01\%$)[17] and comparable to L^B ($Q^{Eu}_L \approx 0.7\%$)[26] or $(L^C\text{-H})^-$ ($Q^{Eu}_L = 1.3\%$).[27]

To confirm the nature of the Eu^{III} chemical environment in LaEu, we have measured its high-resolution laser-excited excitation and emission spectra on both a microcrystalline sample and single crystals and compared them to those of similar samples of EuEu. For LaEu, the $^5D_0 \leftarrow {}^7F_0$ transition, which is unique for a given metal ion environment, appears as a single, symmetrical component centered at 17230 cm^{-1} (full width at half-height (fwhh) 11 cm^{-1}) at 295 K and at 17219 cm^{-1} (fwhh = 7 cm^{-1}) at 10 K, for both samples. In comparison, EuEu also displays a single 0−0 component at 17232 (295 K) and 17221 (10 K) cm^{-1}. At first sight, this may be surprising. However, one has to recall that $[Eu_2(L^A)_3]^{6+}$ is extremely weakly luminescent, 50 times less than $[Eu_2(L^B)_3]^{6+}$, and therefore, the emission from the bpb site will be hardly seen in the presence of the emission from the bpa site. Since X-ray structures of both LaEu and EuEu pointed to HHH helicates, one can conclude that the observed excitation spectrum arises from a Eu^{III} ion coordinated to the bpa ends of the three ligand strands. Analysis of the emission spectra of LaEu under either broad-band or selective laser excitation is consistent with a pseudo-D_3 symmetry for the metal ion (Figure 8, Supporting Information). The faint $^5D_0 \rightarrow {}^7F_0$ transition (0.3% of the total emission intensity) is symmetry forbidden in the D_3 point group.[49] The three observed transitions to the $^7F_1$ level can be labeled $A_1 \rightarrow A_2$ (A_2 at 291 cm^{-1} with respect to $^7F_0$) and $A_1 \rightarrow$ split E

(49) Bünzli, J.-C. G. In *Lanthanide Probes in Life, Chemical and Earth Sciences. Theory and Practice*; Bünzli, J.-C. G., Choppin, G. R., Eds.; Elsevier Science B.V.: Amsterdam, 1989; Chapter 7.

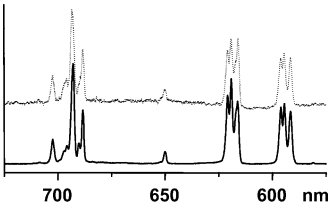

Figure 8. Emission spectra of single crystals of EuEu (top curve) and of a microcrystalline sample of LaEu (bottom curve) at 10 K under ligand excitation (25250 cm^{-1}).

Table 5. Energy (cm^{-1}) of the Identified Crystal-Field Sublevels of the Eu(^7F_j) Manifold ($j = 1-4$) in $[LnEu(L^{AB})_3](ClO_4)_6 \cdot 2H_2O$ (Ln = La or Eu) As Determined from Excitation and Emission Spectra in the Solid State at 10 K under Selective Excitation[a]

	LaEu	EuEu		LaEu	EuEu
$^5D_0$	17219	17221	$^7F_3$	1825	1840
$^7F_1$	291	300	$^7F_4$	2680	2698
	414	409		2733	2737
	430	442		2810	2811
$^7F_2$	974	980		2881	2893
	992	1007		2916	2998
	1051	1054		2993	3019
	1077	1095			
	1122	1119			

[a] $^7F_0$ is taken as the origin.

sublevel (barycenter 422 cm^{-1}). The transitions to $^7F_2$ (two closely split components to the two E sublevels and one unsplit component to the A_1 sublevel) and to $^7F_4$ can also be consistently interpreted in terms of the same distorted D_3 symmetry (Table 5).

Solution Structure: Lanthanide-Induced Shift Analysis. More quantitative information on the solution structure of the heterobimetallic helicates has been extracted from the lanthanide-induced paramagnetic shifts for the series HHH-$[LnLu(L^{AB})_3]^{6+}$ (Ln = Ce, Pr, Nd, Sm, Eu), for which all the ^1H NMR signals could be successfully assigned (Supporting Information). Lanthanide-induced paramagnetic shifts (LISs) for a given Ln^{III} ion j, $\Delta_{i,j}$, are calculated by subtracting for each proton i the chemical shift value of the diamagnetic species LaLu:

$$\Delta_{i,j} = \delta_{i,j} - \delta_{i,La} = (\Delta_c)_{i,j} + (\Delta_p)_{i,j} = F_i\langle S_z\rangle_j + C_j B_0{}^2 G_i \quad (2)$$

where Δ_c and Δ_p are the contact (through bond) and pseudocontact (through space) contributions to the LIS, respectively. They both depend on parameters characteristic of either the paramagnetic Ln^{III} ion (the spin expectation value $\langle S_z\rangle_j$, the second-order magnetic axial anisotropy value for the free ion C_j, and the ligand field parameter $B_0{}^2$) and of the H nucleus (the hyperfine coupling constant F_i and the geometric factor $G_i = (3\cos^2\theta_i - 1)/r_i{}^3$). In the latter, r_i is the Ln(bpb)···H_i distance and θ_i the angle between the Ln(bpb)···H_i vector and the molecular axis, which is taken as the Ln(bpb)−Ln(bpa) vector. In the definition of both quantities, it is assumed that the paramagnetic ion is coordinated by the bpb moiety of the ligand.

The determination of solution structure based on the separation of the contact and pseudocontact contributions is well documented, and we have used both one-proton

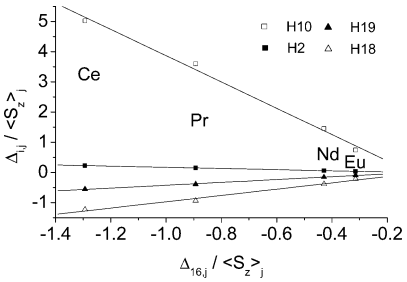

Figure 9. LIS analysis: plots according to the two-proton method for pairs of protons (i, $k = 16$). See the text.

(Reilley) and two-proton (Geraldes) methods[50] to assess whether or not the investigated axial complexes are isostructural in solution. In the latter method, the linear forms of the equations expressing $\Delta_{i,j}$ for two different protons i and k are combined, allowing the elimination of the ligand field parameter:

$$\frac{\Delta_{i,j}}{\langle S_z\rangle_j} = \left[F_i - \left(\frac{G_i}{G_k}\right)F_k\right] + \left(\frac{G_i}{G_k}\right)\frac{\Delta_{k,j}}{\langle S_z\rangle_j} \tag{3}$$

In a first step, eq 3 was fitted to $\Delta_{i,j}$ values (Supporting Information) for LnLu (Ln = Ce, Pr, Nd, and Eu), leaving out SmLu since $\Delta_{i,\mathrm{Sm}}$ values are small and $\langle S_z\rangle_{\mathrm{Sm}}$ difficult to determine theoretically.[51] H16 was used as the reference proton ($k = 16$). Some plots are shown in Figure 9. Utilizing the values of slopes and intercepts found for the CeLu, PrLu, NdLu, and EuLu complexes, LIS values were calculated for SmLu with $\langle S_z\rangle_{\mathrm{Sm}}$ ranging from 0.01 to 0.39. A value of $\Delta_{i,\mathrm{Sm}}$ was calculated for each $\langle S_z\rangle_{\mathrm{Sm}}$ and each proton i, as well as the corresponding agreement factor, $\mathrm{AF}_{\mathrm{Sm}}$:

$$\mathrm{AF}_j = \left[\frac{\sum_i (\Delta_{i,j}^{\mathrm{calcd}} - \Delta_{i,j}^{\mathrm{exptl}})^2}{\sum_i (\Delta_{i,j}^{\mathrm{exptl}})^2}\right]^{1/2} \tag{4}$$

The agreement factors were then plotted as a function of $\langle S_z\rangle_{\mathrm{Sm}}$. An optimal value of $\langle S_z\rangle_{\mathrm{Sm}} = 0.25$ was determined, which has been taken as being appropriate for the SmLu complex and which compares well with data reported in the literature.[51] The results of the analysis on all five helicates, correlation coefficients, slopes (G_i/G_k), and intercepts ($F_i - (G_i/G_k)F_k$) are detailed in the Supporting Information. The correlation is excellent, with almost all coefficients being larger than 0.99, except for H11, whose position close to the so-called "magic angle" ($\theta = 54.74°$) results in small $\Delta_{i,j}$ values and in an unreliable fit. From these data, we conclude that the investigated complexes are isostructural in CD_3CN solution. For the remainder of the analysis the SmLu data were left out since the small $\Delta_{i,j}$ values lower the quality of the fits. The conclusions drawn for the other helicates are, however, assumed to be valid for the SmLu helicate as well.

Contact and pseudocontact contributions have been separated using Reilley's method and eqs 5 and 6.

$$\frac{\Delta_{i,j}}{C_j} = B_0{}^2 G_i + \left(\frac{\langle S_z\rangle_j}{C_j}\right)F_i \tag{5}$$

$$\frac{\Delta_{i,j}}{\langle S_z\rangle_j} = F_i + \left(\frac{C_j}{\langle S_z\rangle_j}\right)G_i \tag{6}$$

Even though the correlation coefficients are not quite as convincingly close to 1 as with the fit utilizing eq 3, the obtained lines are reasonably straight (typical correlation coefficients 0.97−0.99). Contact and pseudocontact contributions to the LIS calculated from the slopes of the two sets of fits are listed in the Supporting Information, and calculated total shifts are compared to the experimental ones in the Supporting Information along with the calculated agreement factors for the individual protons:

$$\mathrm{AF}_i = \left[\frac{\sum_j (\Delta_{i,j}^{\mathrm{calcd}} - \Delta_{i,j}^{\mathrm{exptl}})^2}{\sum_j (\Delta_{i,j}^{\mathrm{exptl}})^2}\right]^{1/2} \tag{7}$$

The agreement factors are satisfactory for all protons with the exception of H11 and H21 because of their position close to the magic angle. Another method of evaluating the quality of the separation is to examine the contact contributions. In the complexes investigated here, it is expected that only protons on the bpb moiety (H10−H23) are topologically close enough to the paramagnetic lanthanide ion to display contact shifts of appreciable magnitude. Indeed this is what is observed for the CeLu and PrLu complexes, with most contact shifts being smaller than 0.1 ppm for protons topologically far away from the lanthanide ion. The separation seems to be less good for the NdLu and EuLu complexes, but that can possibly be ascribed to the small total LIS of these protons, which are both topologically and geometrically distant from the paramagnetic center. On the other hand, the signs of the pseudocontact shifts follow the expected variation in $3\cos^2\theta - 1$, with H11 and H21 being positioned close to the magic angle. The values for the protons on the bpb moiety are qualitatively in good agreement with what was found for complexes of L^1,[39] justifying the use of L^1 as a model for the bpb compartment of L^{AB}. The two methods (Reilley and Geraldes) were compared by recalculating the slopes and intercepts obtained with eq 3 by using parameters obtained from the fits with eqs 5 and 6. As can be seen in the Supporting Information, they yield similar values.

For comparing solution and solid-state structures, the three crystal structures of best quality have been used, i.e., those allowing the determination of the hydrogen positions: LaEu, LaTb, and EuEu. Structural factors (G_i) and ratios (G_i/G_{16}) were calculated from θ_i and r_i values for each ligand strand of each complex (Supporting Information). The agreement

(50) Piguet, C.; Geraldes, C. F. G. C. In *Handbook on the Physics and Chemistry and Rare Earths*; Gschneidner, K. A., Jr., Bünzli, J.-C. G., Pecharsky, V. K., Eds.; Elsevier Science B.V.: Amsterdam, 2003; Chapter 215.
(51) Pinkerton, A. A.; Rossier, M.; Spiliadis, S. *J. Magn. Reson.* **1985**, *64*, 420.

between values obtained from X-ray diffraction and LIS analysis (eq 3) has been quantified by means of the agreement factor defined by eq 8.

$$AF_G = \left[\frac{\sum_{i \neq k} \left(\left(\frac{G_i}{G_k} \right)_{LIS} - \left(\frac{G_i}{G_k} \right)_{X-ray} \right)^2}{\sum_{i \neq k} \left(\left(\frac{G_i}{G_k} \right)_{X-ray} \right)^2} \right]^{1/2} \quad (8)$$

AF_G values were estimated with different subsets of protons, excluding for instance some of the fluxional ethyl groups (Supporting Information). From these considerations, it turns out that the LaTb structure leads to the lowest AF_G factor: 0.166 (all the protons included). This value is low enough to confirm that the LaTb structure determined by X-ray diffraction in the solid state is a good model for the structure in solution, a result in agreement with the relative sizes of the lanthanide ions implied. From this point of view, LaEu and EuEu would indeed be less good models, contrary to PrLu, which should be better, but for which we have no diffraction data of sufficient quality. Removing the ethyl groups from the calculation gives an AF_G value which is slightly smaller (0.149), pointing to the backbone of the ligands in solution being closer to the solid-state conformation than the outer groups. Interestingly, the AF_G values obtained for each of the three individual ligand strands of the LaTb complex are up to 3 times larger than for the averaged structure, demonstrating that a single ligand strand cannot be taken as a good model of the structure in solution. Comparing the AF_G factor for the LaTb structure with the values calculated for the isostructural LaEu and EuEu structures (0.185 and 0.252, respectively) demonstrates how sensitive this agreement factor is to small structural changes.

As a complement to the structural information obtained by LIS analysis, we have measured the longitudinal (spin−lattice) relaxation times (T_1), which yield relative proton−lanthanide distances, for the LnLu helicates in CD_3CN (Ln = La, Ce, Pr, Nd, Sm, Eu). The T_1 data reported in the Supporting Information were determined by means of an inversion−recovery pulse sequence (180°−τ−90°),[52] with 20 values of τ ranging from 10 ms to 10 s. The relaxation times were corrected for diamagnetic effects by subtracting the values measured for the LaLu complex:

$$\frac{1}{T_{1,i}^{para}} = \frac{1}{T_{1,i}^{meas}} - \frac{1}{T_{1,i}^{dia}} \quad (9)$$

As the LIS, the paramagnetic contribution to the spin−lattice relaxation time (often termed lanthanide-induced relaxation, LIR) has two components, through bond and through space. Due to the limited delocalization of the 4f unpaired electron density, the contact term can be ignored for all (weakly covalent) lanthanide complexes. The remaining paramagnetic contributions have been introduced into the simple expression (eq 10)[34,53] for calculating the relative distances; as previously, proton H16 was chosen as the reference.

$$\frac{T_{1,i}^{para}}{T_{1,ref}^{para}} = \left(\frac{r_i}{r_{ref}} \right)^6 \quad (10)$$

Table 6. Relative Ln−H Distances (Reference H16) in $[LnLu(L^{AB})_3]^{6+}$ Helicates, As Determined by LIR Analysis[a]

	r/r_{16}					LaTb, X-ray	
	CeLu	PrLu	NdLu	SmLu	EuLu	mean r	r/r_{16}
H6	1.14	1.17	1.23	1.19	b	7.41	1.16
H8	1.03	1.11	1.07	1.03	b	6.99	1.10
H9	b	1.04	b	b	0.93	6.70	1.05
H9′	b	b	1.16	b	1.13	7.40	1.16
H10	0.64	0.63	0.59	0.62	0.60	3.99	0.63
H12 + H20	1.05	1.09	1.08	b	1.04	6.65	1.04
H13	1.00	1.05	b	b	b	6.46	1.01
H13′	0.86	0.93	0.86	0.85	b	6.10	0.96
H14	1.04	b	1.11	b	1.09	6.27	0.98
H15	0.83	0.87	0.87	b	0.91	5.56	0.87
H16	1.00	1.00	1.00	1.00	1.00	6.38	1.00
H17	0.82	0.87	0.87	b	0.83	5.56	0.87
H18	0.87	0.92	0.92	b	b	6.00	0.94
H18′	0.98	1.04	0.99	0.94	0.86	6.55	1.03
H19	1.14	1.10	b	1.07	1.12	6.96	1.09

[a] Values for H7, H11, H21, H22, and H23 not calculated due to lack of a reference value for the LaLu complex. [b] Not measured due to overlap of lines.

Only protons closer than 8 Å from the paramagnetic lanthanide ion yield reliable distances since diamagnetic contributions dominate for more distant protons, leading to unsatisfactory separation of the paramagnetic contribution. The agreement between relative distances determined by means of LIR analysis in solution and distances determined by X-ray diffraction in the solid state of the LaTb complex is quite good (Table 6), the differences being less than 5% for most protons. This confirms not only the assignment of the ^1H NMR spectra but also the conclusion drawn from the LIS analysis that the structure of the helicates is the same in solution and in the solid state and that LaTb is a reasonable structural model for the investigated LnLu series (Ln = La, Ce, Pr, Nd, Sm, Eu).

Lanthanide Interaction with Ligands L^{AC} and L^{BC}. These ligands were tested first with respect to their behavior in the presence of one lanthanide perchlorate and second in the presence of an equimolar mixture of two lanthanide ions. For solubility reasons, spectrophotometric titrations of the deprotonated ligands with one lanthanide perchlorate have been carried out in methanol, and factor analysis pointed to the formation of 1:1, 1:2, 1:3, 2:2, and 2:3 species (see also the Supporting Information). Data were satisfactorily fitted to the following equations, where L^- is either $(L^{AC}\text{-}H)^-$ or $(L^{BC}\text{-}H)^-$:

$$Ln^{3+} + L^- \leftrightarrows [LnL]^{2+} \ (\log \beta_{11}) \quad (11)$$

(52) Vold, R. L.; Waugh, J. S.; Klein, M. P.; Phelps, D. E. *J. Chem. Phys.* **1968**, *48*, 3831.

(53) Peters, J. A.; Huskens, J.; Raber, D. J. *Prog. Nucl. Magn. Reson. Spectrosc.* **1996**, *28*, 283.

$$Ln^{3+} + 2L^{-} \leftrightarrows [LnL_2]^{+} \ (\log \beta_{12}) \quad (12)$$

$$Ln^{3+} + 3L^{-} \leftrightarrows [LnL_3] \ (\log \beta_{13}) \quad (13)$$

$$2Ln^{3+} + 2L^{-} \leftrightarrows [Ln_2L_2]^{4+} \ (\log \beta_{22}) \quad (14)$$

$$2Ln^{3+} + 3L^{-} \leftrightarrows [Ln_2L_3]^{3+} \ (\log \beta_{23}) \quad (15)$$

Various models were examined, and the best fits were obtained with eqs 11−13 and 15 for $(L^{AC}\text{-H})^{-}$ (model 1), whereas both this model and the set of eqs 12−15 (model 2) gave satisfactory results for $(L^{BC}\text{-H})^{-}$. Data reported in Table 7 represent overall constants, since the various isomers (*fac*, *mer*, HH, HT, HHH, HHT) cannot be distinguished by this method. They show the Eu^{III} bimetallic helicate with $(L^{BC}\text{-H})^{-}$ which bears the strongest coordinating groups, being about 6 orders of magnitude more stable than $[Eu_2(L^{AC}\text{-H})_3]^{3+}$ or $[Eu(L^{AB})_3]^{6+}$, the latter two exhibiting a similar stability. Monitoring the titration in methanol-d_4 by ^{1}H NMR confirms the presence of 1:1 (possibly 2:2), 1:2, and 1:3 complexes, in addition to the bimetallic helicates. For $R = 0.67$ and Ln = La, the monometallic 1:1 and 1:2 complexes coexist with $[Ln_2(L^{AC}\text{-H})_3]^{3+}$, while the concentration of the latter species is too small to be detected for Ln = Lu. In $[La_2(L^{AC}\text{-H})_3]^{3+}$, the three ligand strands are not equivalent and the species is the HHT isomer; all the signals are sharp at room temperature, indicating the absence of P ⇆ M interconversion on the NMR time scale.[40]

Close scrutiny of the aromatic signals generated by the 1:3 species with $(L^{AC}\text{-H})^{-}$ (Supporting Information) reveals that some of them are little or not shifted with respect to the free ligand; they correspond to the protons of the terminal benzimidazole−pyridine moieties pointing to the noncoordination of these units. On the other hand, the shifts experienced by the aromatic protons of the benzimidazole−pyridine−carboxylate (bpc) moieties are comparable to those measured for the 1:3 complexes with the deprotonated monotopic ligand **5**, consistent with $[Ln(L^{AC}\text{-H})_3]$ complexes (Ln = La, Lu) in which the three ligand strands are coordinated through the bpc units (a similar conclusion can be drawn for the 1:1 and 1:2 complexes). Moreover, the three ligand strands are equivalent, and the complexes display a ternary symmetry. At room temperature, the signals assigned to the bpb groups are narrow and well resolved while those from the bpc units are broad, a fact we interpret as reflecting a fast *fac*−*mer* equilibrium on the NMR time scale. At 236 K, the interconversion becomes slow enough to observe distinct signals for each isomer.

On a whole, very similar conclusions can be drawn with respect to the stoichiometry, coordination mode (Supporting Information), and lability of the species with $(L^{BC}\text{-H})^{-}$, except that the presence of a 2:2 species is detected in the case of Lu^{III}.

ESI-MS spectra also clearly show the formation of homo- and heterodimetallic helicates in stoichiometric 1:1:3 Ln:Ln′:L mixtures in acetonitrile between lanthanide(III) perchlorates (10^{-3} M) and the deprotonated ligands: $[Ln_2(ClO_4)_xL_3]^{3+}$ and $[LnLn'(ClO_4)_xL_3]^{3+}$ (Ln = La, Eu; L = $(L^{AC}\text{-H})$ (see Table 1) or $(L^{BC}\text{-H})$; $x = 0, 1$). In addition, species with overall 1:1, 1:2, 1:3, 2:2, and 3:2 stoichiometry are detected. The distribution of the bimetallic helicates, determined by ESI-MS spectrometry, is reported in Table 3. As for L^{AB}, appreciable deviations from the statistical distribution appear, although to a lesser extent, pointing to substantial differences between the ligands. For the LaLu pair, for instance, the heterobimetallic species represents up to 89% of the total helicate concentration in the case of L^{AB} and 79% in the case of $(L^{AC}\text{-H})^{-}$, but only 31% in the case of $(L^{BC}\text{-H})^{-}$. In general, solutions with L^{AB} have the largest excess of heterobimetallic helicate despite the less drastic difference between its two coordinating sites compared to $(L^{AC}\text{-H})^{-}$. The respective amounts of isomers present in solutions containing the latter were determined by ^{1}H NMR. For the LaLu system, it turned out that the major heterobimetallic helicate in 3.5×10^{-3} M stoichiometric solution is HHT-LaLu (∼55−65%). Only one of the two HHT heterohelicates forms, as exemplified by the presence of six singlets in the range 5.2−6.5 ppm with the same intensity (two of them overlapping), and the concentration of the HHH helicate is too low to be detected (Supporting Information). It is likely that two of the ligand strands are bound to the Lu^{III} ion through their carboxylate end. The other main species in solution is the HHT-La_2 homobimetallic helicate (∼35−45%) since again six singlets are observed in the 5.2−6.5 ppm range (two pairs of singlets overlapping). The difficulty in analyzing these spectra, as well as the concentration difference (ESI-MS solutions are about 7 times less concentrated), may explain the discrepancy with the data reported in Table 3 regarding the relative concentration of the homo- versus heterobimetallic species. The main conclusion brought by the NMR data is that the majority of the helicates with $(L^{AC}\text{-H})^{-}$ are in the HHT form.

Discussion

Speciation in Solution. The unsymmetrical, hexadentate and ditopic ligands synthesized have been coded for the simultaneous recognition of two lanthanide ions through self-assembly processes leading to triple-stranded bimetallic helicates with approximate trigonal symmetry and HHH configuration, similarly to L^{A}, L^{B}, and $(L^{C}\text{-2H})^{2-}$. Depending on the ligand (L^{AB}, $(L^{AC}\text{-H})^{-}$, $(L^{BC}\text{-H})^{-}$), the solvent (acetonitrile or methanol), the counterion (perchlorate or triflate), and the initial Ln:L ratio, several different complexes have been evidenced, with Ln:L stoichiometries equal to 1:2, 1:3, 2:3, 1:1, and 2:2. In fact, as with the symmetric ditopic ligands, the recognition of a pair of lanthanide ions is only very effective under stoichiometric conditions. Figure 10 summarizes the percentages of five major species in equilibrium at the stoichiometric ratio (Ln/Ln′ mixtures) and clearly points to L^{AB} being the best host. Since L^{AC} and L^{BC} bear a carboxylic acid function which was deprotonated before the self-assembly process, it was not expected that the change of solvent (methanol versus acetonitrile) would greatly affect the formation of the complexes; indeed, L^{C} builds extremely stable molecular edifices in water. In fact, the carboxylate group has such a high complexation ability

Table 7. Stability Constants Determined at 295 K in Methanol at 295 K for Complexes with Deprotonated Ligands $(L^{AC}\text{-}H)^-$ and $(L^{BC}\text{-}H)^-$ and in Acetonitrile for Complexes with L^{AB}

L	Ln	log β_{11}	log β_{12}	log β_{13}	log β_{23}	log β_{22}
L^{AB}	Eu				23.9 ± 0.5[a]	
$(L^{AC}\text{-}H)^-$	La	7.8 ± 0.2	12.2−13.9[b]	19.0 ± 0.2	24.1−25.3[b]	
	Eu		12.6 ± 0.4	17.9 ± 0.5	23.3 ± 0.7	
	Lu	7.2 ± 0.2	12.2−13.0[b]	17.3 ± 0.1	22.6−24.6[b]	
$(L^{BC}\text{-}H)^-$	Eu	9.3 ± 0.3	15.6 ± 0.3	20.9 ± 0.3	29.8 ± 0.5	
	Eu[c]		15.1 ± 0.4	20.8 ± 0.4	29.7 ± 0.6	22.5 ± 0.6

[a] In acetonitrile. [b] Only a range of values could be determined. [c] Using model 2 (see the text).

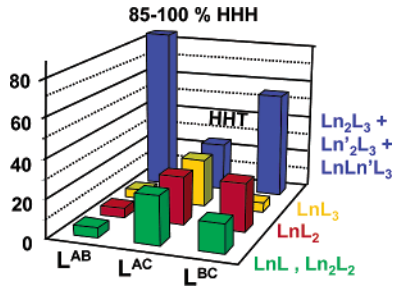

Figure 10. Relative concentrations of complexes observed in stoichiometric solutions Ln:L = 2:3 and Ln:Ln′:L = 1:1:3 in acetonitrile (L = L^{AB}, HHH) or in methanol (L = L^{AC}, L^{BC}, HHT) by ^{1}H NMR spectroscopy and/or determined using the stability constants.

compared to the benzimidazole or carboxamide entities that all lanthanide ions compete for it, preventing the efficient helical wrapping of the three ligand strands around two metal ions, hence the four species with equal concentration evidenced in solutions of $(L^{AC}\text{-}H)^-$. The stability constants log β_{23} of the homobimetallic species $[Ln_2(L^{AC}\text{-}H)]^{3+}$ are not larger than for the $[Ln_2L_3]^{6+}$ helicates (L = L^A, L^B, L^{AB}), which is surprising considering that one moderately, respectively substantially, coordinating tridentate unit is replaced by a much stronger one. Moreover, these constants do not vary significantly between La and Lu, and the triple-stranded helicate is essentially HHT. For $(L^{BC}\text{-}H)^-$, the difference in the complexing strength of the two compartments is somewhat reduced, resulting in a much larger concentration of the target molecules (55%); furthermore, the homobimetallic helicate exhibits a stability 6 orders of magnitude larger compared with $[Eu_2(L^{AB})_3]^{6+}$.

On the other hand, the two compartments of L^{AB} present an adequate difference in complexing ability, leading to both the almost quantitative formation of the bimetallic triple helicates and an appreciable enhancement in the concentration of the heterobimetallic species (∼90%) over the statistical value (50%). Here the proportion of HHH complexes reaches 85−100%, depending on the species, Ln_2, LnLn′, or Ln'_2. The preferential formation of the HHH isomers over the HHT ones is the result of an interplay between two factors. The first one is related to the specific free energy for the complexation of Ln^{III} ions with the two different compartments of the ligand. The second one arises from interstrand interactions which vary with the size of the specific Ln^{III} ion pair and the orientation of the ligand strands. This problem will be addressed in more detail in a subsequent paper.

$[LnLn'(L^{AB})_3]^{6+}$ Helicates: Structural Aspects. The self-assembly process leads to structurally well-defined cavities for the complexation of Ln^{III} ions which lie in a slightly distorted tricapped trigonal prismatic geometry. The extent of the distortion is evidenced both by the analysis of the coordination polyhedra (see above) and in the low-temperature luminescence spectra of the EuEu and LaEu helicates. Indeed, the splitting of the $^7F_1(E)$ sublevel, as revealed by inspection of the $^5D_0 \rightarrow {}^7F_1$ transition (Table 5), is connected to the deviation from the idealized D_3 symmetry. It amounts to $\Delta E_{E-E} = 16$ cm^{-1}, a small value compared to 24 cm^{-1} for $[Eu_2(L^A)_3](ClO_4)_6 \cdot 2H_2O$, 29 cm^{-1} for $[Eu_2(L^B)_3](ClO_4)_6 \cdot 5H_2O$,[26] or 42 cm^{-1} in a related 4f−4f−4f trimetallic helicate.[47] A theoretical approach using the point charge electrostatic model allows approximate correlations between the magnitude and sign of the second-rank crystal-field parameter B_0^2 and the energy difference between the A and E sublevels in trigonal prismatic sites.[54] Here, B_0^2 is negative because A_2 lies at lower energy than the 2-fold degenerate sublevel E, and its absolute magnitude is proportional to ΔE_{E-E}, which is equal to 131 cm^{-1}, a value identical to the one reported for $[Eu_2(L^B)_3](ClO_4)_6 \cdot 5H_2O$.[26] On the other hand, the corresponding splitting for $[Eu_2(L^A)_3](ClO_4)_6 \cdot 2H_2O$ is much smaller, 85 cm^{-1},[17] and the presently reported luminescence data are therefore consistent with the Eu^{III} ion being coordinated to the three bpa ends of the ligand strands.

A bimetallic helicate is characterized by the intermetallic distance and its pitch P,[55] which is the distance needed for the ligands to make a complete turn around the pseudo-C_3 axis going through the two metal centers (Table 7). For instance, in the case of LaEu, a mean rotation of 333.7° is needed to go from O1 to N8 (ligand strand a), from O2 to N17 (ligand stand b), or from O3 to N26 (ligand strand c). The two planes defined by O1, O2, and O3 and N8, N17, and N26 are quasi parallel (interplanar angle 3°), and their distance d amounts to 12.45 Å. The data listed in Table 8 for L^{AB} helicates are estimated from the mean N(benzimidazole)−Ln−Ln′−O(amide) dihedral angle α_{di} and the interplanar distance d: $P = 360(d/\alpha_{di})$, which yields a helical pitch of 13.4 Å for LaEu. We note that the helical pitches for the heterobimetallic helicates are very similar, indicating only minute structural changes along the series. They are slightly longer than the ones calculated for the homobimetallic edifices with the symmetrical ligands L^A, L^B, and L^C, in line with a longer intermetallic distance (by about 0.3 Å).

(54) Görller-Walrand, C.; Binnemans, K. In *Handbook on the Physics and Chemistry of Rare Earths*; Gschneidner, K. A., Jr., Eyring, L., Eds.; Elsevier Science B.V.: Amsterdam, 1996; Vol. 23, Chapter 155.
(55) Piguet, C.; Bernardinelli, G.; Hopfgartner, G. *Chem. Rev.* **1997**, *97*, 2005.

Table 8. Helical Pitches P and Intermetallic Distances $d_{LnLn'}$ in $[LnLn'(L^{AB})_3]^{6+}$ and Corresponding Reference Homobimetallic Helicates[a]

	L^A	L^B	$(L^C\text{-}2H)^{2-}$ [b]		L^{AB}				
	LnLn′ = EuEu	LnLn′ = TbTb	LnLn′ = EuEu	LnLn′ = TbTb	LnLn′ = LaEu	LnLn′ = LaTb	LnLn′ = PrEr	LnLn′ = PrLu	LnLn′ = EuEu
P/Å	12.8	13.0	12.8	13.3	13.5	13.4	13.2	13.2	13.5
$d_{LnLn'}$/Å	8.88	9.06	8.93	8.95	9.21	9.20	9.22	9.21	9.35

[a] Values for L^A, L^B, and $(L^C\text{-}2H)^{2-}$ are recalculated from the corresponding structural data. [b] Average values (the structures feature two slightly different molecules).

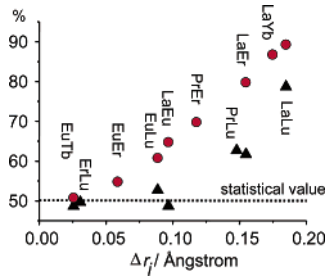

Figure 11. Percentages of heterobimetallic $[LnLn'(L)_3]^{6+}$ ($L = L^{AB}$, circles; $(L^{AC}\text{-}H)^-$, triangles) observed by ESI-MS and/or ^1H NMR in acetonitrile solutions at room temperature, versus the ionic radius differences.

Interpretation of NMR spectra and LIS analysis show the solid-state structure being maintained in acetonitrile, leading to well-defined and fairly rigid coordination cavities, hence the long and almost temperature-independent Eu($^5D_0$) lifetime, which represents an asset in the design of luminescent probes.

Recognition of Lanthanide Heteropairs. The main interest of this paper lies in L^{AB} (and to a lesser extent L^{AC}) being able to recognize a heteropair of lanthanide ions and to insert them into a stable triple helical functional edifice by self-assembly. In a first approximation, the chemical properties of Ln^{III} ions may be related to their ionic radius and charge density. We have therefore plotted in Figure 11 the percentages of heterobimetallic species as a function of the ionic radius difference Δr_i for a coordination number of 9. When Δr_i is larger than 0.1 Å, the proportion of heterospecies with L^{AB} becomes larger than 65%, which is not the case for $(L^{AC}\text{-}H)^-$, for which $\Delta r_i > 0.15$ Å is needed to reach a similar value. The recognition process may be quantified considering the following equation:

$$[LnLn(L^{AB})_3]^{6+} + [Ln'Ln'(L^{AB})_3]^{6+} \leftrightarrows 2[LnLn'(L^{AB})_3]^{6+} \quad (K, \Delta G_r)$$

$$\Delta(\Delta G) = \Delta G_r - \Delta G_{stat} \qquad (16)$$

At room temperature, a statistical distribution results in $K_{stat} = 4$ and $\Delta G_{stat} = -3.4$ kJ·mol^{-1}. The increased stability of the $[LnLn'(L^{AB})_3]^{6+}$ helicates with respect to the homobimetallic ones, expressed as $\Delta(\Delta G)$ defined by eq 16, is reported in Table 3. The absolute free energy values steeply increase between $\Delta r_i = 0.1$ Å and $\Delta r_i = 0.18$ Å, from ~3 to ~10 kJ·mol^{-1} (90% heterobimetallic species). These energies remain small, and very weak differences in thermodynamic and entropic contributions, e.g., interstrand $\pi-\pi$ or C−H···π interactions (~2−8 kJ·mol^{-1}),[56] account for this stabilization. We note that such interactions also favor the HHH arrangement of the ligand strands. The better discriminating effect displayed by L^{AB} compared to $(L^{AC}\text{-}H)^-$ can precisely be traced back to the preferential formation of the HHH isomers with the former ligand. Looking at the formation of the helical monometallic complexes with ligand L^1 and its 4-pyridine-substituted analogues,[39] we see that a size-discriminating effect along the Ln^{III} series principally occurs upon complexation of the third ligand strand, because the key factor in the recognition process is the size of the self-assembled cavity. In the case of HHT bimetallic helicates, the three tridentate coordination units are not identical and the resulting cavity is different from those built by the tridentate ligands, hence a less pronounced size-discrimination effect.

(56) Hunter, C. A.; Sanders, J. K. M. *J. Am. Chem. Soc.* **1990**, *112*, 5525.

Conclusion

In the initial design of the ditopic ligands presented here, we expected that the variable affinity of their coordinating units versus the lanthanide ion sizes would lead to the selective incorporation of two different metal ions into triple-stranded bimetallic helicates. Two among the three tested ligands effectively lead to selective supramolecular recognition of heteropairs of lanthanide ions. However, contrary to our initial thoughts, the best host, by far, proved to be neutral L^{AB} and not deprotonated L^{AC}. This finding is important since it points to the selectivity being governed by a combination of electrostatic interactions and interstrand interactions. We indeed observe that L^{AB} forms a majority of HHH helicates, which is by far not the case for $(L^{AC}\text{-}H)^-$, and a high selectivity is precisely related to this configuration of the complexes. Altogether, remarkable enhancements of the concentration of the heterobimetallic $[LnLn'(L^{AB})_3]^{6+}$ species over the statistical distribution are obtained when the ionic radius differences are larger than 0.1 Å, reaching up to 90% for the LaLu pair. In terms of energy, this translates into differences in ΔG_r (with respect to the statistical situation) remaining modest, between −3 and −10 kJ·mol^{-1}, hence the difficulty in planning the adequate ligands. The data reported in this paper shed light on the subtle origins of the selectivity and demonstrate that a good understanding of them allows chemists to master the design of ingenious hosts leading to bimetallic functional edifices.

Our final goal is the design of bifunctional probes featuring either two-color luminescence or luminescence and magnetic properties. From this standpoint, the supramolecular edifices described here are promising: the heterobimetallic helicates are highly stable and kinetically inert, and the lanthanide ions are well protected from outside interactions. To produce practical probes, several improvements need however to be implemented in the ligand design, such as water solubility,

better antenna effect (the quantum yield of 1.9 % for LaEu is nevertheless comparable to the one exhibited by the commercially used $[Eu(bpy{\cdot}bpy{\cdot}bpy)]^{3+}$ cryptate[9]), and substitution by a group able to couple with biological material. The feasibility of the latter has already been demonstrated with a symmetrical ditopic ligand,[57] and experiments are in progress in our laboratory to address the other points.

Altogether, the remarkable disposition of ligand L^{AB} to self-assemble with a heteropair of lanthanide ions opens entirely new perspectives in the design of lanthanide-containing bifunctional edifices and is an exciting example of a multifaceted recognition process.

(57) Tripier, R.; Hollenstein, M.; Elhabiri, M.; Chauvin, A.-S.; Zucchi, G.; Piguet, C.; Bünzli, J.-C. G. *Helv. Chim. Acta* **2002**, *85*, 1915.

Acknowledgment. This research is supported through grants from the Swiss National Science Foundation. We thank Véronique Foiret and Frédéric Gumy for their help in recording the luminescence data.

Supporting Information Available: Experimental details, additional tables and figures, and crystallographic data in CIF format. This material is available free of charge via the Internet at http://pubs.acs.org.

IC0351996